Theor Chem Acc (2012) 131:1256
DOI 10.1007/s00214-012-1256-1

REGULAR ARTICLE

High-pressure studies on azido-tetrazole chain–ring conversion in crystalline 2-azido-4,6-dichloro-1,3,5-triazine

Yan Liu · Li Zhang · Guixiang Wang · Lianjun Wang · Xuedong Gong

Received: 11 April 2012 / Accepted: 9 July 2012 / Published online: 25 July 2012
© Springer-Verlag 2012

Abstract First-principle calculations have allowed us to gain insight into the high-pressure effect on the azide-tetrazole chain–ring conversion of crystalline 2-azido-4,6-dichloro-1,3,5-triazine in the range of 0–90 GPa. The local density approximation with Ceperley-Alder exchange–correlation potential parameterized by Perdew and Zunger has been adopted. With the increase in pressure, the unit cell lattice parameters (*a*, *b*, and *c*), molecular geometries (bond lengths, interatomic distance, and bond angles), atom charges, bond populations, band gap, and density of states change gradually and regularly except at 13, 47, and 59 GPa due to the structural transformation. The azido angle reaches to the maximum at 12 GPa and then bends to 170.76° at 13 GPa, but the azido group is approximately linear. From 47 GPa, the azido group loses the linearity and bends evidently. When the pressure is boosted to 59 GPa, the azido group cyclizes completely and a five-membered tetrazole ring is built, that is, the azide-tetrazole chain–ring conversion occurs. This tetrazole structure keeps unchanged under higher pressures till 90 GPa. The volumes of unit cell and densities vary stably, and no obvious discontinuity happens owing to the structural transformation, while a small discontinuity appears in the total energy at 59 GPa. The calculated thermodynamic functions suggest that the azide-tetrazole conversion may be facile to progress according to the fundamentals of chemical thermodynamics.

Keywords 2-Azido-4,6-dichloro-1,3,5-triazine · High pressure · First-principle calculation · Azide-tetrazole chain–ring conversion

Y. Liu (✉) · G. Wang · L. Wang (✉) · X. Gong (✉)
School of Chemical Engineering, Nanjing University of Science and Technology, Nanjing 210094, Jiangsu, People's Republic of China
e-mail: yanliu_nanjing@yahoo.com.cn

L. Wang
e-mail: wanglj@mail.njust.edu.cn

X. Gong
e-mail: gongxd325@mail.njust.edu.cn

L. Zhang · L. Wang
School of Environmental and Biological Engineering, Nanjing University of Science and Technology, Nanjing 210094, People's Republic of China

1 Introduction

Organic azides have extensive applications in many fields. Some azides are potential explosive substances and have been used in armament industry, and some are effective precursors for carbon nitride nanomaterials [1–6]. Even the antiviral drug azidothymidine (AZT), used for the treatment of HIV/AIDS, also contains an azido group [7]. And they are also capable of a great diversity of organic reactions and popular for participation in click chemistry [8–13].

When the azido group is attached to a C atom adjacent to a nitrogen in a heterocyclic azide, it may spontaneously cyclize to give a tetrazole ring [14], namely, azido-tetrazole chain–ring isomerization, which has been the subject of many studies. There are abundant experimental and theoretical studies concerning this isomerization [15–29], but these studies mainly performed in solutions, the gas phase, or in the melt. The transformation induced by the high pressure in the crystal has been little reported up to now.

As is well known, high-pressure technique, as an investigation method, has been applied extensively to study

various materials [30–39]. It may cause polymorph transitions and induce some new and unexpected phases that are generally inaccessible at the ambient pressure or normal condition. When subjected to high pressure, almost any material will be compressed into a denser form. For example, coesite and stishovite, two denser forms of quartz, were first discovered in high-pressure experiments and later found in nature at the site of a meteor impact [40]. Another example is man-made synthetic diamond, which was first produced when applying high pressure as well as high temperature to carbon [41–43]. In our former study on 2-diazo-4,6-dinitrophenol (DDNP), we found DDNP molecule exists in the quinoid form when the pressure is below 10 GPa, but it has the cyclic azoxy form as the pressure is above 10 GPa [44]. We are also interested in high-pressure studies on the azide-tetrazole chain–ring conversion in nitrogen-containing heterocyclic azide. In this study, 2-azido-4,6-dichloro-1,3,5-triazine (ADCT) is chosen as the researching object due to its potential application in organic photochemistry and photobiology as well as nanomaterials [45–48].

As compared with the high-pressure experimental methods [49, 50], computational methods have competitive advantages since they allow a wide range of pressures to be explored relatively easily and have the potential to provide detailed information under extreme conditions, which is often difficult to obtain from experiment for practical reasons. First-principle periodic calculations have been performed using density functional theory (DFT) [51, 52] to study the effect of high pressure on the structure and phase transformation in many materials [53–57]. DFT is a powerful, formally exact theory and capable of accurate results at low cost. But as a computational approach, it also has some limitations. For example, the geometry optimization is in good agreement with the experiment, but it cannot catch all possible phase transformation with regard to molecular dynamics simulation. Moreover, local density approximation (LDA) within DFT scheme over-binds materials and accordingly predicts larger cohesive energies, equilibrium bulk moduli, and smaller equilibrium lattice parameters than experimental data. Though generalized gradient approximation (GGA) is an improvement upon the LDA in principle, it does not necessarily lead to improved results in practice. It generally tends to produce better cohesive energies, but it will overcorrect lattice parameters and bulk moduli to the extent; accordingly, the agreement is worse than LDA due to the consequence of error cancellation [58, 59]. DFT calculations often fail to describe dispersive molecular crystals with weak van der Waals interaction; nevertheless, some studies have testified that DFT results of weakly bound molecular systems are improved under high pressures, where there is substantial overlap of electronic densities from various molecules [60–64]. Dispersion correction plays little effect on the trend of structural change with the increasing pressure. Hence, DFT has been performed in this manuscript to study the effect of high pressure on the azido-tetrazole chain–ring conversion in crystalline ADCT.

2 Computational methods

In this study, first-principles calculations for crystalline ADCT were performed using the CASTEP code [65] within the DFT formalism. The initial crystal structure adopted the experimental crystalline structure in Ref. [66]. ADCT crystallizes in the orthorhombic space group *Pbca* with $a = 7.465$ Å, $b = 9.526$ Å, and $c = 20.016$ Å and contains 88 atoms per unit cell as shown in Fig. 1. The LDA with Ceperley-Alder exchange–correlation potential [67] parameterized by Perdew and Zunger [68] (CA-PZ) was employed. The Vanderbilt-type ultrasoft pseudopotential [69] and a plane-wave expansion of the wave functions were used for geometry optimization. The electronic wave functions were obtained within the Pulay density-mixing scheme [70], and the structures were optimized with the BFGS method [71]. The cutoff energy of plane waves was set to 400.0 eV to ensure the convergence of total energies. Brillouin zone sampling was performed by using the Monkhost–Pack scheme with a *k*-point grid of $3 \times 2 \times 2$. Periodic nature of the crystal has been considered by using periodic boundary conditions in three directions. The full optimization of the structure was performed to allow the atomic positions, cell shape, and volume to change. During the geometry relaxation, the total energy of the system was converged to less than 5.0×10^{-6} eV, the residual force less than 0.01 eV/Å, the displacement of atoms less than 5.0×10^{-4} Å, and the residual bulk stress less than 0.02 GPa. The external stress was exerted from *x*, *y*, and *z* directions, equivalent to hydrostatic pressures. Similar calculations were carried out under different external stresses of 0–90 GPa to study the pressure effect on the geometrical and electronic structures of ADCT.

The Mulliken atom charges, bond populations, band structure, densities of states, and phonon spectra were calculated and analyzed based on the optimized structure. Based on the calculation results of phonon spectra, the vibrational contributions to the thermodynamic properties can be evaluated, and accordingly, the temperature dependence of the thermodynamic functionals such as enthalpy (H), entropy (S), free energy (G), and lattice heat capacity (C_p) of a crystal can be computed in a quasi-harmonic approximation. These results can be used to predict phase stability of different structural modifications or phase transitions.

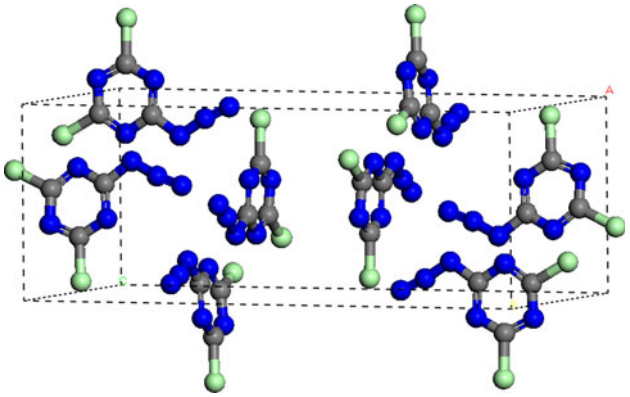

Fig. 1 The experimental unit cell of ADCT

3 Results and discussion

To benchmark the performance of the theoretical approaches, both LDA and GGA were applied to the bulk ADCT as a test. For GGA, the Perdew–Burke–Ernzerhof (PBE) [72], Perdew–Wang-91 (PW91) [73], and Wu-Cohen (WC) [74] functionals were chosen. The unit cell lattice parameters obtained with LDA/CA-PZ, GGA/PBE, GGA/PW91, and GGA/WC at ambient pressure without any constraint, along with the experimental data for ADCT, are presented in Table 1. The mean relative errors of lattice parameters for the four methods are −3.86, 8.52, 8.75, and 8.51 %, respectively. Obvious, the deviation of LDA results is the smallest, that is, the LDA/CA-PZ results agree better with the experimental ones than those of GGA. This is also the case for bond lengths and angles. This shows LDA can successfully predict the structure and properties of ADCT crystal, and it is employed in this study.

3.1 Pressure effect on crystal structure and energy

The increase in pressure can cause evident changes in the unit cell magnitude. The relaxed lattice parameters (a, b, c), unit cell volume (V), density (ρ), and total energy (E_{tot}) of ADCT crystal under different hydrostatic pressures are depicted in Fig. 2.

When the pressure increases from 0 to 12 GPa, a, b, and c decrease obviously, but c decreases most, that is, the compressibilities along three directions are not tantamount, which indicates that the compressibility of ADCT crystal is anisotropic. When the pressure of 13 GPa is applied, a and b decrease suddenly, while c increases sharply. In the pressure range of 13–46 GPa, a, b, and c shorten a little gradually, but when the pressure reaches to 47 GPa, the regular variation trend has been broken again. c decreases sharply, while a and b increase a little. Then a, b, and c shorten slightly and gradually with the increasing pressure. Unusual changes occur the third time at 59 GPa. c increases and b decreases suddenly, a remains little changed. After that, a, b, and c keep on varying regularly until 90 GPa. Under all hydrostatic compressions, the crystal symmetry maintains the same orthorhombic space group *Pbca* as the experimental one.

Though the declining tendencies of a, b, and c with the increasing pressure have been destroyed at 13, 47, and 59 GPa, V and ρ varies regularly as the pressure increases. Comparatively, the change in V and ρ is more pronounced in the low-pressure range than in the high-pressure range.

The total energy of the unit cell (E_{tot}) rises successively with the increasing pressure except at 59 GPa, which indicates that the intermolecular interactions increase as the molecules approach to each other. In addition, as compared with a, b, c, V, and ρ, E_{tot} rises linearly with the increasing pressure except the small discontinuity at 59 GPa. The good linear relationship between E_{tot} and P can be shown from the correlation coefficient (R) 0.9931.

3.2 Pressure effect on molecular geometry

The increase in pressure causes obvious changes in not only the unit cell but also the molecular geometries. High pressure will induce the molecular conformation changes or structural transformation supposing the molecule has some conformational flexibility, which leads to phase transitions and the formation of more densely packed materials. To illuminate the effect of pressure on the molecular geometry, especially the azide-tetrazole ring-chain isomerism, firstly, the experimental molecular geometry and atomic numbering of ATAN are depicted in Fig. 3. And some main geometrical parameters such as

Table 1 Comparison of the lattice constants obtained with LDA/CA-PZ, GGA/PBE, GGA/PW91, and the experimental data for ADCT at ambient pressure

	a	re$_a$	b	re$_b$	c	re$_c$	me
CA-PZ	7.094	−4.97	9.455	−0.75	18.840	−5.87	−3.86
PBE	7.701	3.17	10.512	10.35	22.426	12.04	8.52
PW91	7.751	3.83	10.515	10.38	22.426	12.04	8.75
WC	7.690	3.02	10.520	10.44	22.431	12.06	8.51
Exp	7.465		9.526		20.016		

re the relative error of the calculated values to the experimental ones, given in percentage, *me* the average error of the absolute relative ones

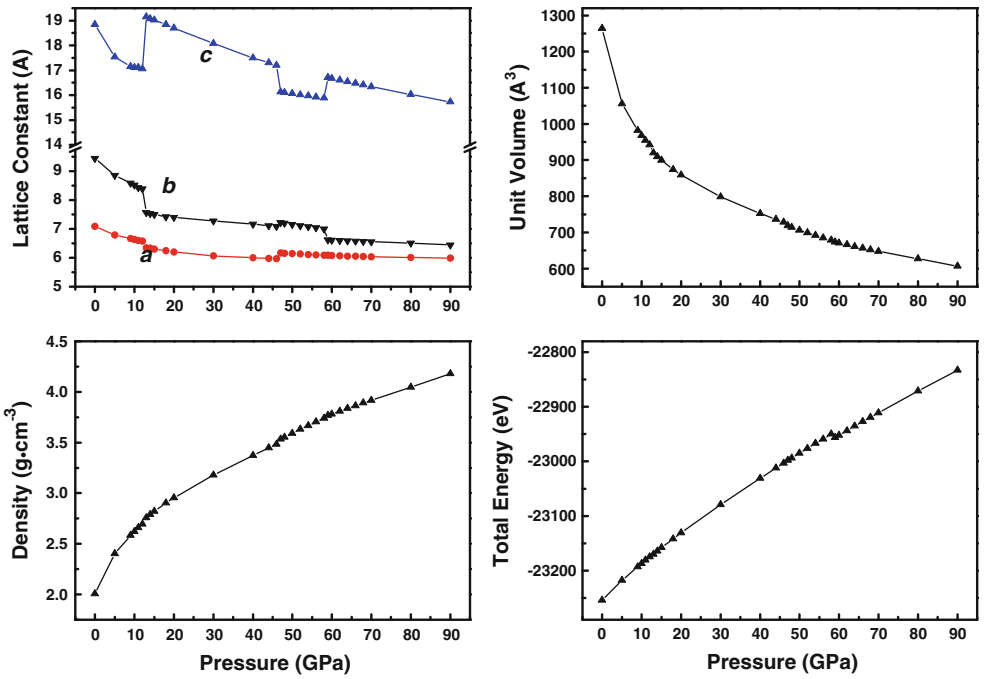

Fig. 2 The optimized lattice parameters (*a*, *b*, *c*), unit cell volume, density, and total energy as functions of pressure

bond lengths and bond angles at various pressures are presented in Figs. 4 and 5. Figure 4a gives the variations of the lengths of bonds involved directly with the azide-tetrazole transformation with the pressure. Figure 4b provides the lengths of other five bonds in triazine ring with the pressure. Figure 5 presents the variation of bond angles N7–N8–N9, C2–N7–N8, N1–C2–N7, and N8–N9–N1, respectively. The perspective views of ADCT molecule at different pressures are displayed more intuitionistically and visually in Fig. 6.

With the pressure increasing from 0 to 12 GPa, all bonds shorten gradually, and the interatomic distances between N1 and N9 are above 3.0 Å; thus, ADCT molecule exists in the azido chain isomer. Though the azido group is described as linear, bond angle N7–N8–N9 is not absolute but close to 180°. The experimental value of N7–N8–N9 in ADCT crystal is 171.98°, and its calculated value gradually increases from 171.57° at 0 GPa to the maximum 177.10° at 12 GPa. But when the pressure reaches 13 GPa, the angle decreases again to 170.76°, and all bonds change unusually, which results in the jumps in bond lengths, angles, and lattice parameters (*a*, *b*, and *c*).

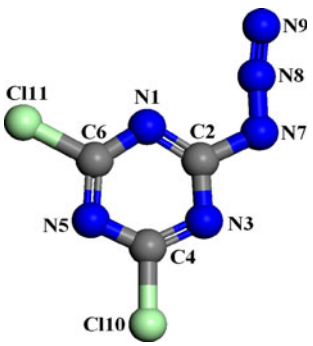

Fig. 3 The experimental molecular geometry and atomic numbering of ATAN

From 13 to 46 GPa, all bonds shorten gradually, while the bond angles (N7–N8–N9, N1–C2–N7, and C2–N7–N8) vary indistinctively as compared with bond lengths. When the pressure reaches to 47 GPa, the regular variation trend has been broken again. Besides the loss of linearity of the azido group, which bends about 16°, all bonds lengthen or shorten unusually. This discontinuity is also reflected in *a*, *b*, and *c*. From 47 to 58 GPa, the angle N7–N8–N9 bends further, and interatomic distance N1–N9 and bonds N1–C2, C2–N7, N3–C4, C4–N5, N5–C6, and C6–N1 shorten, while N7–N8, N8–N9, and C2–N3 lengthen steadily. In the whole, the bending of the azido group (N7–N8–N9) goes with the increase in the length of N7–N8 and N8–N9 and decrease in that of C2–N7.

When the external pressure increases to 59 GPa, there are remarkable changes in molecular geometry. The azido group bends further about 28°, and the angle N7–N8–N9 reaches 110.42° Accordingly, the angle N8–N9–N1 varies from 80.18° to 106.78°, and angles N1–C2–N7 and C2–N7–N8 also adjust to 108.11° and 107.01°. The corresponding angles in crystalline 5-methyl-1H-tetrazole are 110.58°, 106.20°, 107.42°, and 106.43°, respectively [75]. The very close data show azido chain converts to tetrazole ring at 59 GPa. Furthermore, all covalent bonds vary

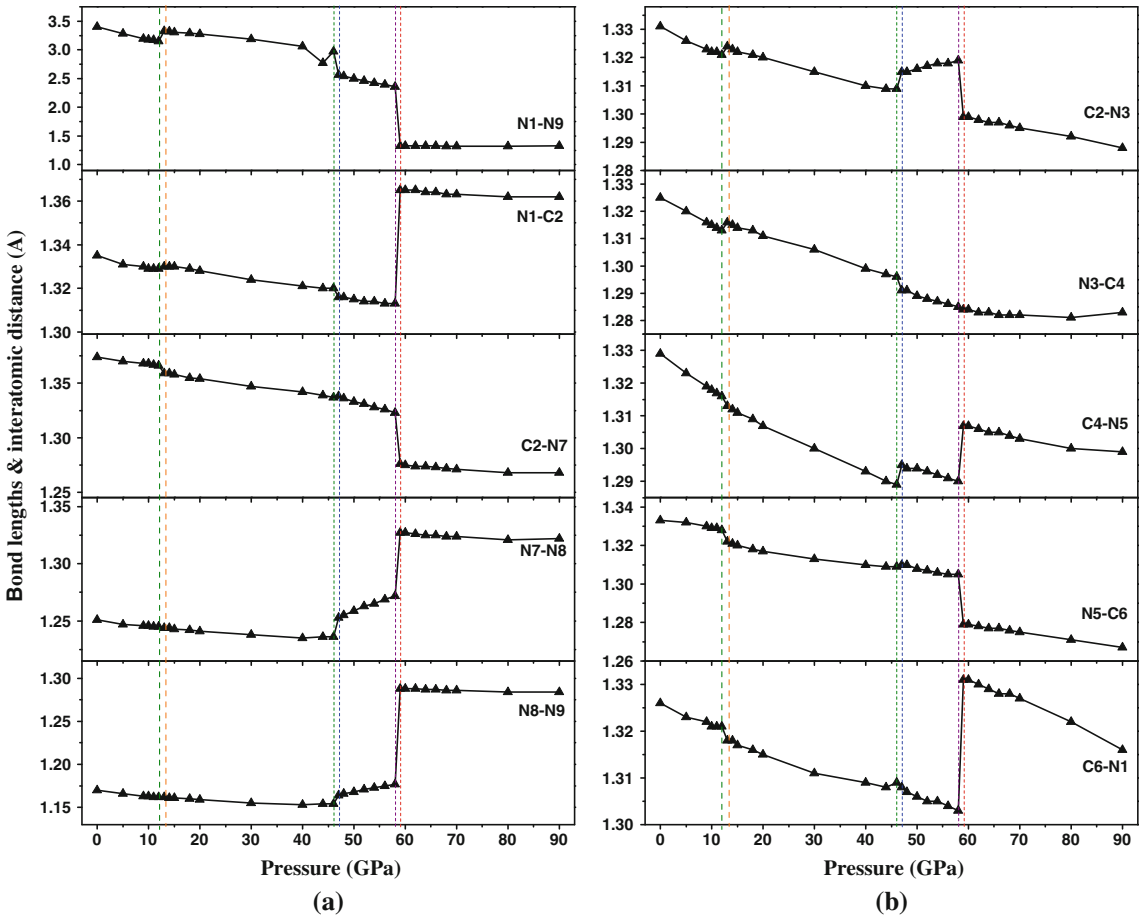

Fig. 4 Variation of the bond lengths and interatomic distances between N1 and N9 with pressure

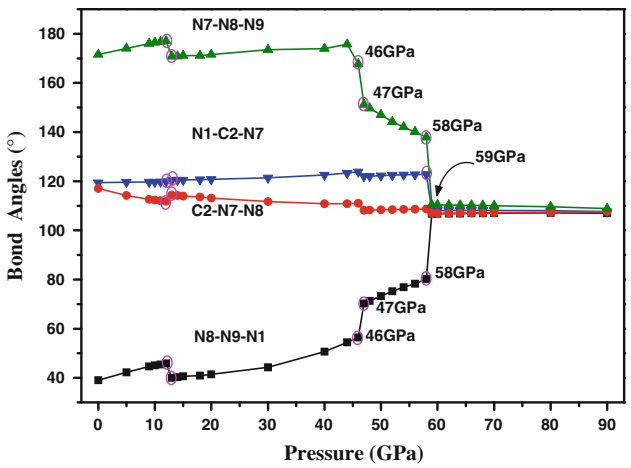

Fig. 5 Variation of the bond angles with pressure

evidently, but the changes in the bonds upon cyclization are much larger than those other five bonds in triazine ring, for example, the bond N8–N9 elongates 0.11 Å, the other three bonds N7–N8, C2–N7, and N1–C2 all vary 0.05 Å, while the bonds in the triazine ring vary below 0.03 Å. Of course, the most relevant bond change upon cyclization concerns the interatomic distance N1–N9. It decreases suddenly from 2.358 Å at 58 GPa to 1.327 Å at 59 GPa, which indicates that a covalent bond between N1 and N9 generates and tetrazole ring forms. The large change in molecular structure at 59 GPa caused larger discontinuity in *a*, *b*, and *c* than those at 13 and 47 GPa. In addition, the only small discontinuity in E_{tot} at 59 GPa is presumably due to the ring closure to form the tetrazole ring at this pressure.

When the pressure increases further till 90 GPa, the bond angles and bond lengths in the tetrazole ring keep almost unchanged, which shows the higher pressure has little influence on the tetrazole ring; however, the bonds in the triazine ring vary more obviously.

3.3 Pressure effect on electronic structure

3.3.1 Atom and bond populations

To gain insight into the effect of pressure on the redistribution of electron density in the cyclization, the variations of atom charges and bond populations with pressure are examined. After inspection of the atom charges, it has been found that pressure may affect the electron density

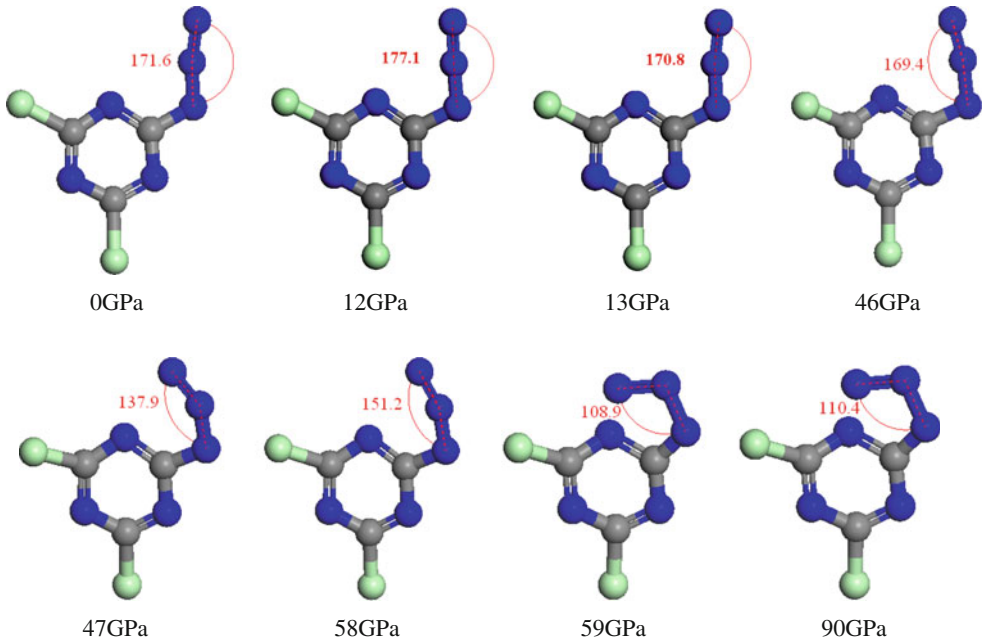

Fig. 6 Perspective views of ADCT molecule at different pressures

redistribution, but the most of redistribution occurs at the pressure 59 GPa where the azido chain converts to tetrazole ring. Figure 7 depicts the variation trends of the atomic charges of N1, N8, and N9 with pressure for crystalline ADCT.

In the pressure range below 40 GPa, the atomic charges remain little affected; hence, no evident structural change in ADCT occurs. When higher pressure is applied, especially at 47 GPa, the negative charge on N1 and the positive one on N8 and N9 all decrease. And on this occasion, the azido group begins bending. The largest changes in charge occur at 59 GPa, where the negative charge on N1 decreases substantially from −0.42 e to −0.12 e, and the charge on N8 varies from 0.16 e at 58 GPa to −0.11 e at 59 GPa, while the change in N9 is only 0.04 e. This means that the charges transfer from N1 to N8 via N9 and azide chain is converted to tetrazole ring. Under the pressure higher than 59 GPa, the atom charges change slightly, which also suggests high pressure can promote the increase in the delocalization degree of electrons.

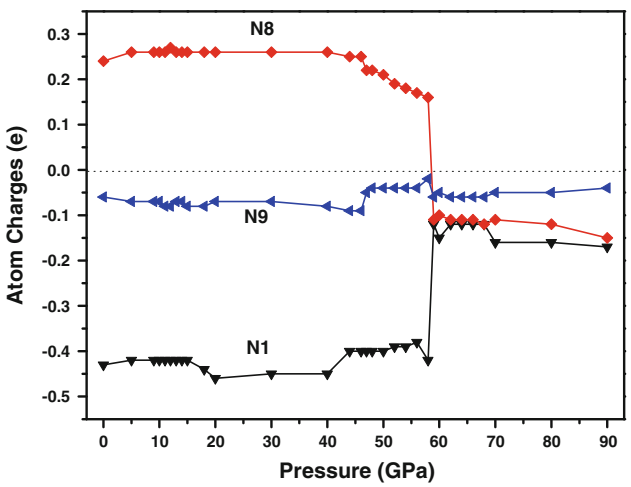

Fig. 7 The atomic charges of N1, N8, and N9 in ADCT at different pressures

Figure 8 shows the bond populations of the bonds, whose bond lengths have been depicted in Fig. 5, under different pressures for ADCT. Usually, the higher the bond population, the more covalent character the bond is [76]. As can be seen, the most noteworthy change in population occurs from 58 to 59 GPa for all bonds. The change at N1–N9 ranks the first, increasing sharply from about 0 to 0.77. The second largest change is at N8–N9, about 0.38. The populations of N1–C2 and C2–N7 decrease or increase about 0.22 and those of N5–C6 and C6–N1 increase or decrease about 0.12, while that of N7–N8 is affected very little. Hence, bending of the azido group through the angle N7–N8–N9 at 59 GPa promotes electron transfer from the bond N8–N9 to N1–N9, concomitant with the initial attack of the lone pair on N1 to the azido group, leading to the formation of the covalent bond between N1 and N9. This is also reflected the charge transfer from N1 to N8 via N9. Moreover, the changes in bonds related to azido-tetrazole conversion are notably larger than those in triazine ring.

3.3.2 Band structure

Based on the equilibrium crystal structures obtained at different pressures, the self-consistent band structures

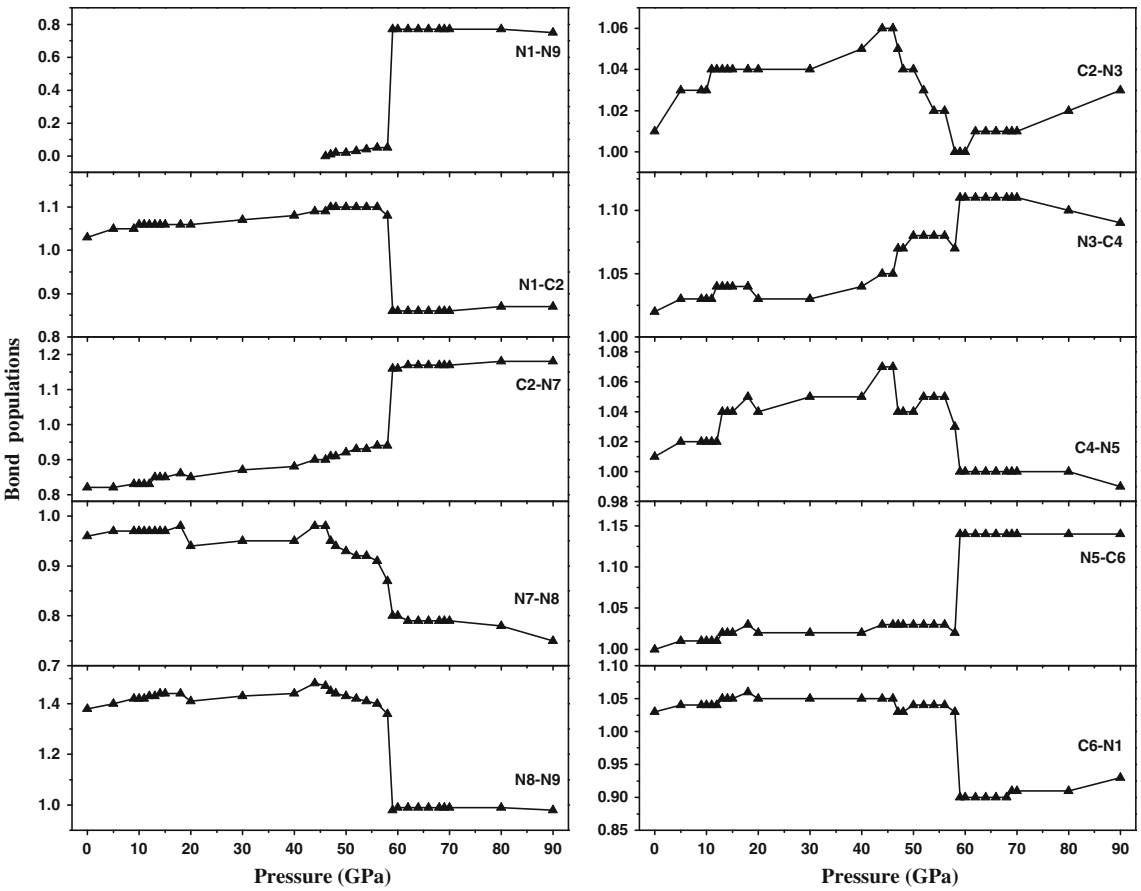

Fig. 8 Variation of the bond populations as a function of pressure

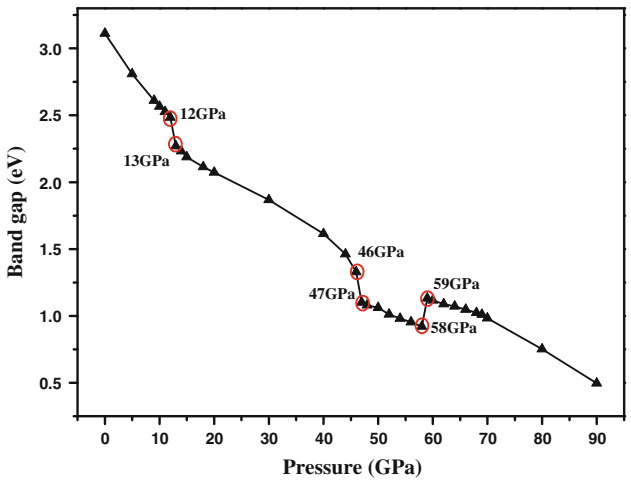

Fig. 9 Band gap of solid ADCT as a function of pressure

along different symmetry directions of the Brillouin zone have been calculated at different pressures. The energy gap (ΔE_g) between the highest occupied crystal orbital (HOCO) and the lowest unoccupied crystal orbital (LUCO), an important parameter to characterize the electronic structure of a solid and is related to its sensitivity, can be obtained. Though all DFT methods, in particular, LDA, underestimate the band gap, which can be corrected by introducing an empirical scissors correction, this does not affect the variation trend of the band gap of crystal with the increasing pressure. The calculated ΔE_g of ADCT as a function of pressure is shown in Fig. 9. Within the pressure range of 0–58 GPa, ΔE_g decreases gradually with the pressure increasing. It is because the decrease in intermolecular space under compression leads to an increase in electron overlap between molecules in the system. This shows that the probability of electron transitions from the occupied valence bands to the empty conduction bands increases. According to principle of the easiest transition (PET) of electrons [77], the decrease in band gap may lead to the decrease in the stability of the material as the pressure increases. As can also be seen, the average decrease rate of ΔE_g in different pressure ranges is quite different. The average decrease rate is only 0.052 eV/GPa from 0 to 12 GPa and 0.024 eV/GPa from 13 to 40 GPa. Two largest decreases rate occur from 12 to 13 GPa, about 0.215 eV/GPa and from 46 to 47 GPa, about 0.227 eV/GPa. This difference in the ΔE_g reduction may be resulted from the

different compressibility degree of the ADCT crystal in different pressure region. When the pressure turns into 59 GPa, ΔE_g augments dramatically to 1.131 eV due to the azido-tetrazole transformation of ADCT molecule. This also suggests that tetrazole isomer is stabler than azido form.

3.3.3 Density of states

An analysis of densities of states (DOS) is helpful to understanding the changes in electronic structure caused by external pressure. Some characteristics such as the width of the valence band, the energy gap, and the number and intensity of the main peaks can be used to qualitatively interpret experimental spectroscopic data. The calculated DOS for crystalline ADCT at different pressures are presented in Fig. 10. Obviously, the higher the pressure, the lower and wider the peaks are. When the pressure is low, the curves of DOS are characterized by distinct peaks, but with increasing pressure, the peaks widen and the band dispersion increase gradually, consequently, electronic delocalization in bulk ADCT increases. And there is a tendency of shifting to the lower energy in the conduction bands with the increasing pressure. This leads to a reduction in the band gap and shows that the electronic nonlocality gradually increases with the increasing pressure, which is consistent with the conclusion drawn from the analysis of band gap. When the pressure is 90GPa, the DOS becomes a little smooth and DOS in each energy region is approximately close, that is, the probabilities of electron appearance in different energy levels are comparable.

Partial density of states (PDOS) shows which atoms in the system contribute electronic states to various parts of the energy spectrum by resolving these contributions according to the angular momentum of the states. PDOS analyses give a qualitative handle on the nature of electron hybridization in the system and the origin of the main feature peaks in XPS and optical spectra. The atom-resolved PDOS of DDNP at 46, 47, 58, and 59 GPa are shown in Fig. 11. The essential difference between those at 46 and 47 GPa is that the largest contribution to the lower conduction bands is from the p states of C atoms in the triazine ring in the former and the N atoms in the azido group in the latter, respectively. At 58 GPa, the upper valence bands are predominated by the p states of the N atoms in triazine ring, and the lower conduction bands are mainly contributed from the p states of N atoms in azido group. While at 59 GPa, the N states in azido group contribute more for the upper valence bands, and the C states in triazine ring mainly make up the lower conduction

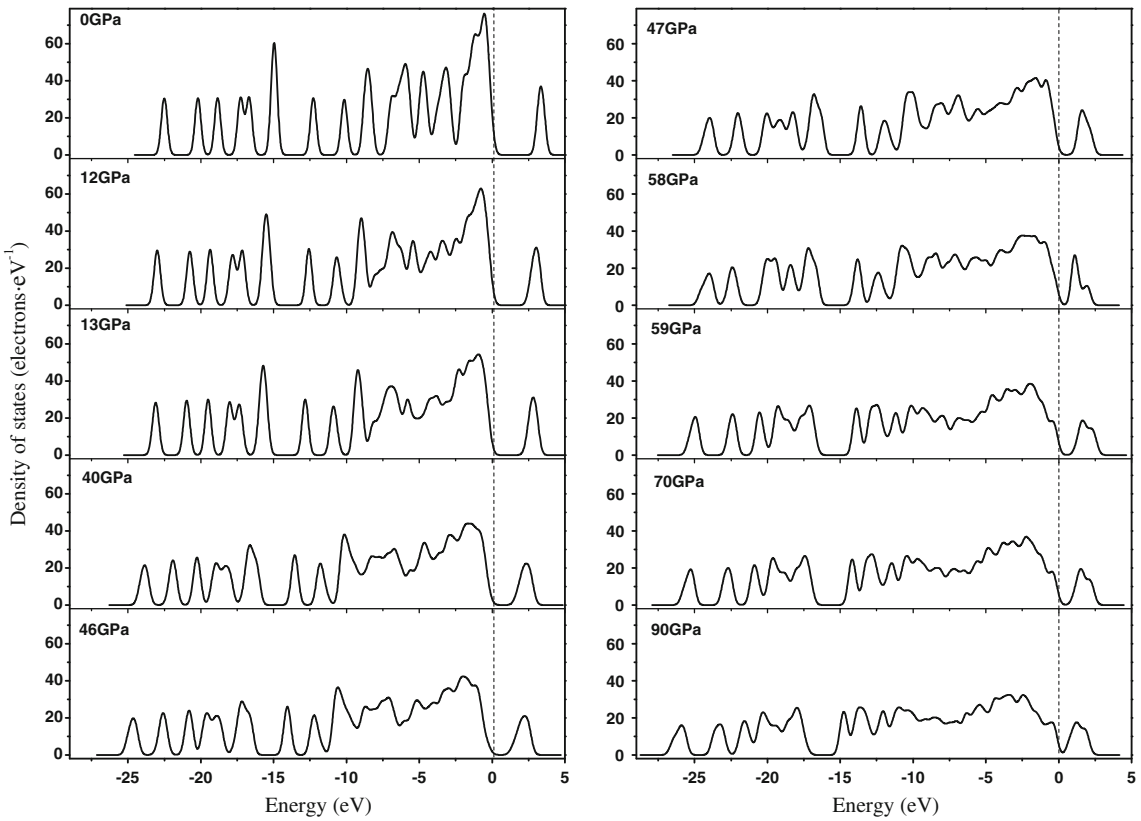

Fig. 10 Calculated total DOS for bulk ADCT at different pressures; S, p, and total states are shown as *dot*, *dash*, and *solid curves*, respectively

bands. Furthermore, the N states in azido group move toward the Fermi level and overlap that of N atom in triazine ring. This indicates hybridization occurs between the N atoms in ring and $-N_3$ group according to the principle of energy matching; thus, the azido group cyclizes and the five-membered tetrazole ring forms.

3.4 Thermodynamic properties

The calculated thermodynamic functions including enthalpy (H), entropy (S), free energy (G), and heat capacity (C_p) as a function of temperature for crystalline ADCT at 58 and 59 GPa are displayed in Fig. 12. Obviously, H, S, and C_p of the solid ADCT increase monotonically with the increase in temperature. This is because the weak translational and rotational motions of the molecules are the main contributions to these three thermodynamic functions at lower temperature, whereas the vibrational motion is intensified and makes more contributions to them at higher temperature. But the variation tendency of free energy (G) is opposite to those of H, S, and C_p, which indicates that the $T \times S$ term increases more rapidly than the enthalpy term since $G = H - T \times S$.

It can also be seen that H and G at 59 GPa are larger than those at 58 GPa at the same temperature. This is because the high-pressure compression results in the increase of intermolecular interactions and corresponding increase of the unit cell energy. Free energy change (ΔG) for crystalline ADCT from 58 to 59 GPa at 298.15 K is 15.72 kJ mol^{-1}. Such small ΔG suggests the azide-tetrazole conversion may be facile to progress according to the fundamentals of chemical thermodynamics. But for S and C_p, the values at 58 GPa is a little larger than those at 59 GPa, that is, the entropy decreases in the azide-tetrazole conversion, in agreement with the loss of degrees of freedom upon cyclization.

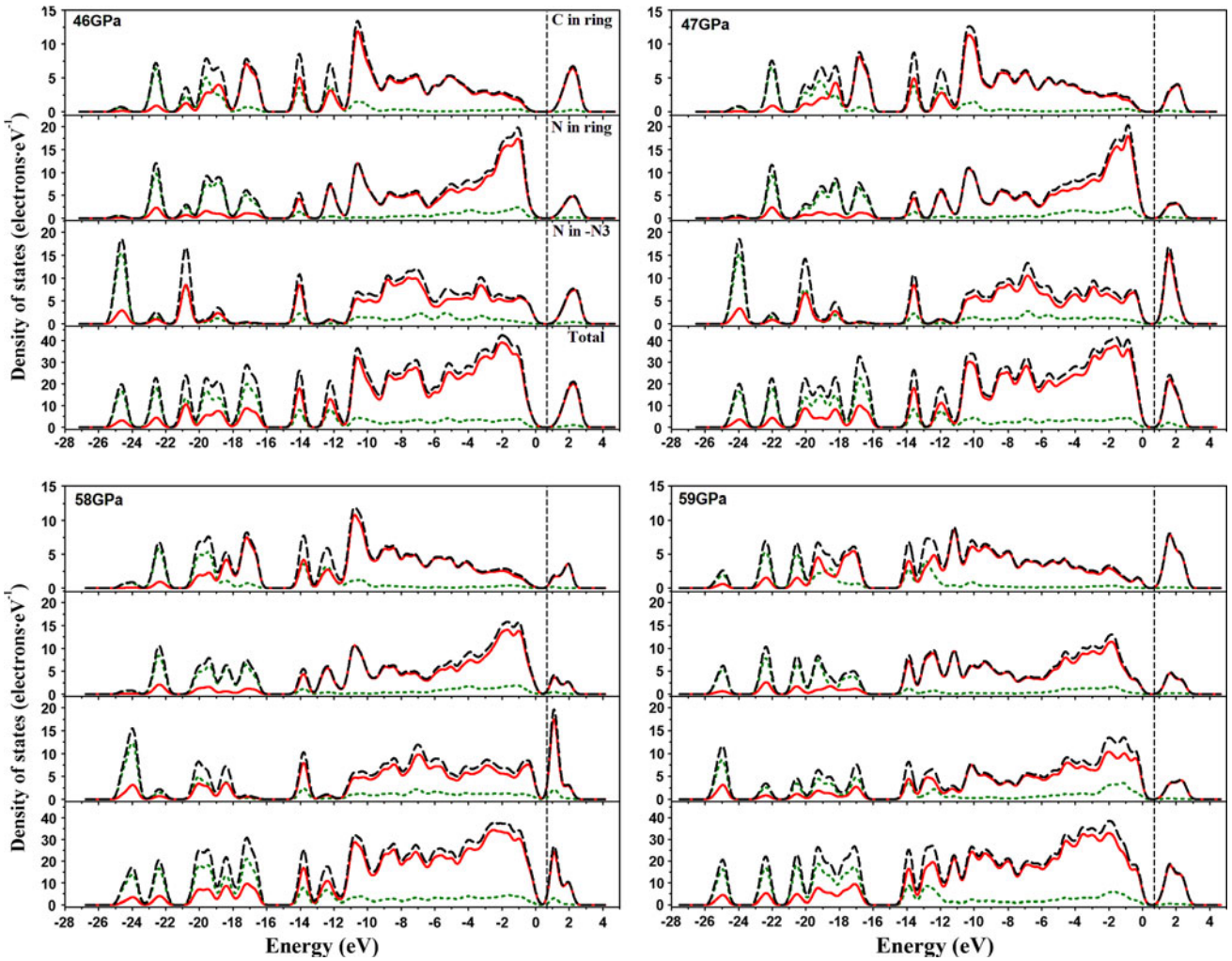

Fig. 11 PDOS of ADCT at 46, 47, 58, and 59 GPa; S, p, and total states are shown as *dot*, *dash*, and *solid curves*, respectively

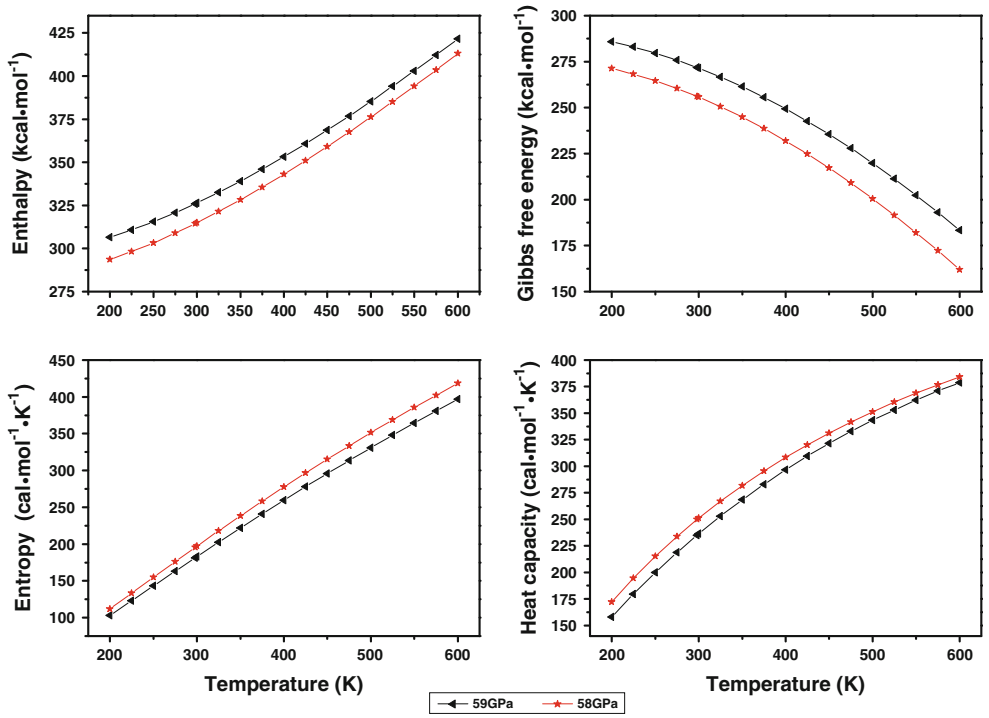

Fig. 12 The thermodynamic functions as a function of temperature for crystalline ADCT at 58 and 59 GPa

4 Conclusions

In this study, periodic ab initio calculations have allowed us to gain insight into the high-pressure effect on the azide-tetrazole chain–ring conversion of crystalline 2-azido-4,6-dichloro-1,3,5-triazine in the range of 0–90 GPa.

The gradual increase in external pressure causes the regular variation in molecular geometry with the pressure increasing from 0 to 12 GPa, all bonds shorten gradually, and angle N7–N8–N9 gradually increases from 171.57° at 0 GPa to the maximum 177.10° at 12 GPa. But when the pressure reaches 13 GPa, the angle decreases again to 170.76°, and all bonds change unusually. From 13 to 46 GPa, all bonds lengths and angles vary regularly, while the regular variation trend has been broken again at 47 GPa. The azido group bends obviously (about 16°) and all bonds lengthen or shorten unusually. From 47 to 58 GPa, the azido group bends further, and all bonds vary steadily. When the pressure increases to 59 GPa, the interatomic distance between N1 and N9 (1.327 Å) and the bond angles (about 108°) indicate a new bond N1–N9 generates and tetrazole ring forms, that is, azido chain converts to tetrazole ring. When the pressure increases further till 90 GPa, the bond angles and bond lengths in the tetrazole ring keep almost unchanged, while the bonds in the triazine ring vary more obviously.

The variations of atomic charges and the bond populations for ADCT molecule with pressure agree well with those of geometries, which further verify the azido-tetrazole conversion. The lattice parameters a, b, and c decrease gradually with the increasing pressure except at 13, 47, and 59 GPa where structural transformations occur. Though the declining tendencies of a, b, and c with the increasing pressure have been destroyed at 47 and 59 GPa, V and ρ varies regularly as the pressure increases. The total energy (E_{tot}) of the unit cell rises successively with the increasing pressure except at 59 GPa. The good linear relationship between E_{tot} and P can be shown from the correlation coefficient (R) 0.9931.

In addition, the band gap deceases gradually except at 13, 47, and 59 GPa due to the molecular transformations. The DOS analysis shows that the electronic delocalization increases under the influence of pressure. The thermodynamic functions suggest that the azide-tetrazole conversion may be facile to progress according to the fundamentals of chemical thermodynamics and the entropy decreases upon this cyclization.

Maybe this work will provide useful information in understanding the high-pressure effect on the azide-tetrazole chain–ring conversion and may offer enhanced opportunities to discover some new structures of ADCT that are generally inaccessible at the ambient pressure.

Acknowledgments We gratefully thank the National Natural Science Foundation of China (Grant No. 11076017) and the Major Project of Water Pollution Control and Management Technology of China (No. 2012ZX07101-003-001) for the support of this work.

References

1. Cantillo D, Gutmann B, Kappe CO (2011) J Am Chem Soc 133:4465–4475
2. Bräse S, Gil C, Knepper K, Zimmermann V (2005) Angew Chem Int Ed 44:5188–5240
3. Miller DR, Swenson DC, Gillan EG (2004) J Am Chem Soc 126:5372–5373
4. Chavez DE, Hiskey MA, Gilardi RD (2000) Angew Chem Int Ed 39:1791–1793
5. Jaidann M, Roy S, Abou-Rachid H, Lussier LS (2010) J Hazard Mater 176:165–173
6. Ye C, Gao H, Boatz JA, Drake GW, Twamley B, Shreeve JM (2006) Angew Chem Int Ed 45:7262–7265
7. Camerman A, Mastropaolo D, Camerman N (1987) Proc Natl Acad Sci 84:8239–8242
8. Moses JE, Moorhouse AD (2007) Chem Soc Rev 36:1249–1262
9. Blackman ML, Royzen M, Fox JM (2008) J Am Chem Soc 130:13518–13519
10. Spiteri C, Moses JE (2010) Angew Chem Int Ed 49:31–33
11. Hoyle CE, Bowman CN (2010) Angew Chem Int Ed 49:1540–1573
12. Boren BC, Narayan S, Rasmussen LK, Zhang L, Zhao H, Lin Z, Jia G, Fokin VV (2008) J Am Chem Soc 130:8923–8930
13. Himo F, Lovell T, Hilgraf R, Rostovtsev VV, Noodleman L, Sharpless KB, Fokin VV (2005) J Am Chem Soc 127:210–216
14. Kessenich E, Polborn K, Schulz A (2001) Inorg Chem 40:1102–1109
15. Burke LA, Elguero J, Leroy G, Sanala M (1976) J Am Chem Soc 98:1685–1690
16. Cubero E, Orozco M, Luque FJ (1998) J Am Chem Soc 120:4723–4731
17. Deev SL, Shenkarev ZO, Shestakova TS, Chupakhin ON, Rusinov VL, Arseniev AS (2010) J Org Chem 75:8487–8497
18. Alkorta I, Blanco F, Elguero J, Claramunt RM (2010) Tetrahedron 66:2863–2868
19. Alkorta I, Blanco F, Elguero J (2010) Tetrahedron 66:5071–5081
20. Lioux T, Gosselin G, Mathé C (2003) Eur J Org Chem 3997-4002
21. Abu-Eittah RH, Taha F, Hamed MM, El-Kelany KE (2009) J Mol Struct: Theochem 895:142–147
22. Katrusiak A, Skierska U, Katrusiak A (2005) J Mol Struct 751:65–73
23. Kanyalkar M, Coutinho EC (2000) Tetrahedron 56:8775–8777
24. Dabbagh HA, Lwowski W (2000) J Org Chem 65:7284–7290
25. Lakshman MK, Singh MK, Parrish D, Balachandran R, Day BW (2010) J Org Chem 75:2461–2473
26. Dias M, Mornet R, Laloue M (1995) Bioorg Med Chem 3:361–366
27. Monajjemi M, Honarparvar B, Monajemi H (2006) J Mex Chem Soc 50:143–148
28. Hanoun JP, Faure R, Galy JP, Elguero J (1996) J Heterocyclic Chem 33:747–750
29. Zheng W, Wong NB, Liang X, Long X, Tian A (2004) J Phys Chem A 108:840–847
30. Hall HT (1958) Science 128:445–449
31. Fabbiani FPA, Pulham CR (2006) Chem Soc Rev 35:932–942
32. Patterson JE, Dreger ZA, Gupta YM (2007) J Phys Chem B 111:10897–10904
33. Lipinska-Kalita KE, Pravica MG, Nicol M (2005) J Phys Chem B 109:19223–19227
34. Pravica M, Shen YR, Quine Z, Romano E, Hartnett D (2007) J Phys Chem B 111:4103–4108
35. Dreger ZA, Gupta YM (2007) J Phys Chem B 111:3893–3903
36. Ciezak JA, Jenkins TA, Liu ZX, Hemley RJ (2007) J Phys Chem A 111:59–63
37. Millar DIA, Marshall WG, Oswald IDH, Pulham CR (2010) Cryst Rev 16:115–132
38. Dong ZH, Beilby NG, Huang YN, Song Y (2008) J Chem Phys 128:074501–074509
39. Ricardo IC, Leonardo CPL, Samuel PHR (2010) J Mol Struct 970:51–58
40. Flörke OW, Graetsch HA, Brunk F, Benda L, Paschen S, Bergna HE, Roberts WO, Welsh WA (2008) Ullmann's Encyclopedia of Industrial Chemistry. Wiley-VCH, Weinheim
41. Bovenkerk HP, Bundy FP, Hall HT, Strong HM, Wentorf RH (1959) Nature 184:1094–1098
42. Hazen RM (1999) The diamond makers. Cambridge University Press
43. Reza A, Zhu H, Clarke C (2005) Diam Relat Mater 14:1916–1919
44. Liu Y, Gong XD, Wang LJ, Wang GX (2011) J Phys Chem C 115:11738–11748
45. Oliva CG, Laza PG, Ocariz CO (2011) In: Alvarez-Builla J, Vaquero JJ, Barluenga J (eds) Modern heterocyclic chemistry, vol 1. Wiley-VCH Verlag GmbH & Co KgaA, Weinheim
46. Bucher G, Lenci F, Horspool W (2003) CRC handbook of organic photochemistry and photobiology, vol 1 & 2, 2nd edn. CRC Press, Boca Raton
47. Glaser J, Tragl S, Meyer HJ (2005) Z Krist 220:214–217
48. Schmidt CL, Jansen M (2010) J Mater Chem 20:4183–4192
49. Boldyreva E, Dera P (2010) High-pressure crystallography: from fundamental phenomena to technological applications. Springer Science Business Media BV, Dordrecht
50. Jeanloz R, Celliers PM, Collins GW, Eggert JH, Lee KKM, McWilliams RS, Brygoo S, Loubeyre P (2007) PNAS 104:9172–9177
51. Hohenberg P, Kohn W (1964) Phys Rev B 136:864–871
52. Kohn W, Sham LJ (1965) Phys Rev A 140:1133–1138
53. Byrd EFC, Rice BM (2007) J Phys Chem C 111:2787–2796
54. Zhu WH, Zhang XW, Wei T, Xiao HM (2009) Theor Chem Acc 124:179–186
55. Hu A, Larade B, Abou-Rachid H, Lussier LS, Guo H (2006) Prop Explos Pyrotech 31:355–360
56. Zerilli FJ, Kuklja MM (2007) J Phys Chem A 111:1721–1725
57. Zerilli FJ, Kuklja MM (2006) J Phys Chem A 110:5173–5179
58. Juan Y, Kaxiras E (1993) Phys Rev B 48:14944
59. Dal Corso A, Pasquarello A, Baldereschi A, Car R (1996) Phys Rev B 55:1180
60. Mujica A, Rubio A, Muñoz A, Needs RJ (2003) Rev Mod Phys 75:863–912
61. Liu H, Zhao JJ, Wei DQ, Gong ZZ (2006) J Chem Phys 124:124501–124510
62. Qiu L, Zhu WH, Xiao JJ, Xiao HM (2008) J Phys Chem B 112:3882–3893
63. Wu CJ, Yang LH, Fried LE, Quenneville J, Martinez TJ (2003) Phys Rev B 67:235101
64. Zhu WH, Shi CH, Xiao HM (2009) J Mol Struct Theochem 910:148–153
65. Clark SJ, Segall MD, Pickard CJ, Hasnip PJ, Probert MJ, Refson K, Payne MC (2005) Z Kristallogr 220:567–570
66. Gibson K, Tragl S, Meyer HJ (2005) Z Anorg Allg Chem 631:1751–1752
67. Ceperley DM, Alder BJ (1980) Phys Rev Lett 45:566–569
68. Perdew JP, Zunger A (1981) Phys Rev B 23:5048–5079
69. Vanderbilt D (1990) Phys Rev B 41:7892–7895
70. Kresse G, Furthmüller J (1996) Phys Rev B 54:11169–11186
71. Fischer TH, Almlof J (1992) J Phys Chem 96:9768–9774
72. Perdew JP, Burke K, Ernzerhof M (1996) Phys Rev Lett 77:3865–3868
73. Perdew JP, Wang Y (1992) Phys Rev B 45:13244–13249

74. Wu Z, Cohen RE (2006) Phys Rev B 73:235116
75. Ohno Y, Akutsu Y, Arai M, Tamura M, Matsunaga T (1999) Acta Cryst C55:1014–1016
76. Segall MD, Shah R, Pickard CJ, Payne MC (1996) Phys Rev B 54:16317–16320
77. Xiao HM, Li YF (1995) Sci China Ser B 38:538–545